INTERNATIONAL JOURNAL FOR NUMERICAL METHODS IN FLUIDS
Int. J. Numer. Meth. Fluids 2004; **44**:313–330 (DOI: 10.1002/fld.640)

Numerical simulations of a filament in a flowing soap film

D. J. J. Farnell[1], T. David[2,*,†] and D. C. Barton[3]

[1]*Imaging Science and Biomedical Engineering (ISBE), University of Manchester, Manchester M13 9PT, U.K.*
[2]*Department of Mechanical Engineering, University of Canterbury, Private Bag 4800 Christchurch, New Zealand*
[3]*School of Mechanical Engineering, University of Leeds, Woodhouse Lane, Leeds LS2 9JT, U.K.*

SUMMARY

Experiments concerning the properties of soap films have recently been carried out and these systems have been proposed as experimental versions of theoretical two-dimensional liquids. A silk filament introduced into a flowing soap film, was seen to demonstrate various stable modes, and these were, namely, a mode in which the filament oscillates and one in which the filament is stationary and aligns with the flow of the liquid. The system could be forced from the oscillatory mode into the non-oscillatory mode by varying the length of the filament. In this article we use numerical and computational techniques in order to simulate the strongly coupled behaviour of the filament and the fluid. Preliminary results are presented for the specific case in which the filament is seen to oscillate continuously for the duration of our simulation. We also find that the filament oscillations are strongly suppressed when we reduce the effective length of the filament. We believe that these results are reminiscent of the different oscillatory and non-oscillatory modes observed in experiment. The numerical solutions show that, in contrast to experiment, vortices are created at the leading edge of the filament and are preferentially grown in the curvature of the filament and are eventually released from the trailing edge of the filament. In a similar manner to oscillating hydrofoils, it seems that the oscillating filaments are in a minimal energy state, extracting sufficient energy from the fluid to oscillate. In comparing numerical and experimental results it is possible that the soap film does have an effect on the fluid flow especially in the boundary layer where surface tension forces are large. Copyright © 2004 John Wiley & Sons, Ltd.

KEY WORDS: fluid/structure interaction; flexible filament; soap films

INTRODUCTION

Experiments concerning the properties of soap films have recently been carried out [1–3] and these systems have been proposed as the experimental versions of theoretical two-dimensional

*Correspondence to: T. David, Department of Mechanical Engineering, University of Canterbury, Private Bag, 04800 Christchurch, New Zealand.
†E-mail: tim.david@canterbury.ac.nz

Contract/grant sponsor: EPSRC; contract/grant number: GR/M35154

Received 15 October 2002
Accepted 18 August 2003

liquids. Indeed, we note that particularly interesting fluidic properties were observed when a silk filament was introduced into the flowing soap film [1]. The filament was seen to demonstrate stable modes, which were, namely: a mode in which the filament oscillates; and one in which the filament is stationary and aligns with the flow of the liquid. It was also seen that the system could be forced from the oscillatory mode into the non-oscillatory mode by reducing the length of the filament. In this article we use numerical and computational techniques in order to simulate the coupled behaviour of the filament and the fluid and thereby investigate the complex behaviour of fluid/structure interaction.

We wish to illustrate our approach by choosing a specific case in which the filament is seen to oscillate continuously for the duration of our simulation and preliminary results for this system are presented here. We find that the filament oscillations are strongly suppressed when the effective length of the filament is reduced and we believe that these results are reminiscent of the different oscillatory and non-oscillatory modes observed in the experiments of Zhang *et al.* in Reference [1]. However, our numerical studies indicate that vortices are created at the leading edge, in a similar fashion to the Kármán vortex street emanating from a cylinder, which are then preferentially enhanced along the length of the filament. These vortices are then convected downstream from the trailing edge of the filament, thus providing a vortical structure whose sign changes with each 'flap' of the filament.

THEORY AND NUMERICAL METHOD

In order to describe the underlying theory and our solution procedure, this section is divided into three sub-sections. The first subsection describes the fluid flow equations, whereas the second subsection describes the formulation for the solid filament. The final subsection provides a description of the fluid/structure interaction algorithm.

Fluid flow equations

We assume that the fluid is incompressible, with a viscosity that is Newtonian in form, and that the density is constant. We use similar assumptions to those utilised in experiments for measuring the viscosity of soap films [4]. The flow is treated as being isothermal and laminar, and an argument for this assumption is given below. The relevant time-dependent equations are thus given by

$$\frac{D\tilde{\mathbf{u}}}{Dt} = -\frac{1}{\rho}\nabla\tilde{p} + \nu\nabla^2\tilde{\mathbf{u}} \tag{1}$$

Here $\tilde{\mathbf{u}} = \{\tilde{u}, \tilde{v}\}$ is the 2D vector field corresponding to the x- and y-directions, $\tilde{p}$ is the fluid pressure, ρ is the density of the fluid, and ν is the kinematic viscosity of the fluid. We non-dimensionalise this equation by choosing a characteristic length L (chosen to be the length of the filament) and characteristic velocity U_∞ (U_∞ is the maximum velocity at the inlet to 2D fluid domain), and hence we may write

$$x = \frac{\tilde{x}}{L}; y = \frac{\tilde{y}}{L}; u = \frac{\tilde{u}}{U_\infty}; v = \frac{\tilde{v}}{U_\infty}; t = \frac{\tilde{t}U_\infty}{L}; p = \frac{\tilde{p}}{\rho U_\infty^2} \tag{2}$$

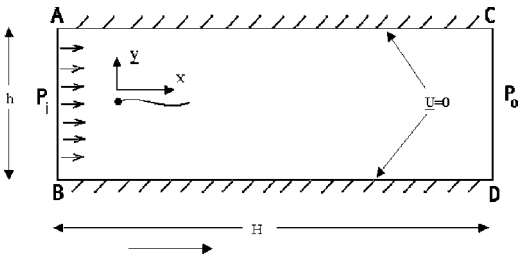

Figure 1. The computational fluid domain. Note that no-slip boundary conditions are imposed on the fluid mesh edges AC and BD and that the motion of the filament is imposed on the fluid as a moving boundary condition.

Equation (1) now becomes

$$\frac{D\mathbf{u}}{Dt} = -\nabla p + Re^{-1}\nabla^2\mathbf{u} \tag{3}$$

with a Reynolds number given by $Re = LU_\infty/v$. The flow domain, shown in Figure 1, consists of a simple 2D rectangular area whose non-dimensional length is H and width h. For the cases presented by Zhang *et al.* [1], the viscosity is given in terms of a surface viscosity and as such the authors calculate a large Reynolds value of approximately 4.5×10^4. Examination of the flow shows clearly that the flow is not turbulent, which would normally be expected at such a high Reynolds number. However Ruttgers *et al.* [2] provide a relationship between the 'surface viscosity' and the more frequently found bulk '3D' value. Indeed, we note that this relationship implies that the Reynolds number is of the order of 10^2 and hence the flow is assumed laminar.

The momentum equations given by Equation (3) are solved using a commercial finite-element code FIDAP. However the code allows a moving boundary constraint to be applied within the computational domain. It is important to realise that this moving boundary condition is generated by the position and velocity of the flexible filament, which are themselves determined via solution of the filament Euler–Lagrange equations (see below.) These constraints may thus be applied and released as a function of time and position for various nodal degrees of freedom. In this present example, the constrained degrees of freedom are simply the two co-ordinate non-dimensional velocities, $\mathbf{u} = \{u, v\}$. The finite-element algorithm uses four-noded linear quadrilateral elements. Velocity is represented linearly, whereas pressure is stored at the element centre as a piece-wise discontinuous function. This ensures stability as well as being able to represent a solid within the fluid domain (as shown in Figure 1).

In order to simulate the 2D soap film flow, we impose no-slip boundary conditions on the top and bottom sides (denoted AC and BD, respectively) of the computational domain as shown in Figure 1. The inlet (AB) has imposed a pressure boundary condition P_i and similarly for the outlet (CD) P_o. The pressure difference $P_\mathrm{i} - P_\mathrm{o}$ is set to ensure that the maximum (non-dimensional) velocity found at the inlet is of order 10°, which agrees with our procedure of non-dimensionalization. There is also a 'no-slip' condition on the filament surface, which corresponds to imposing the fluid vector field to be equal to the filament velocity vector at all nodes 'inside' the filament, this is described in more detail in the section on fluid/structure interaction algorithm.

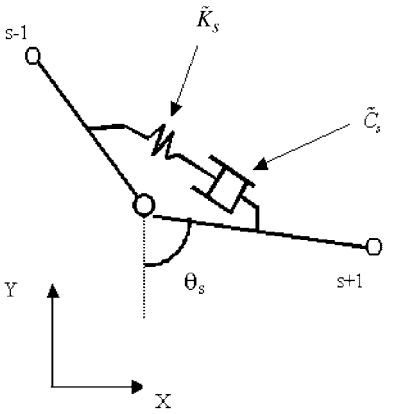

Figure 2. Representation of the $(s-1)$th and sth element of the 'pendulum.' Note that each element has a stiffness coefficient, K_s, and a damping coefficient, C_s, associated with it.

Filament equations of motion

We assume that the filament is of total length L and has total mass is M. Furthermore, we assume that it is composed of N equal length, homogeneous, filament elements. Thus, each element is of length $\tilde{l} = L/N$ and of mass $\tilde{m} = M/N$. The elements are fixed to one another at their hinge (or fulcrum) points. The whole filament (or flag) is thus assumed to be approximated by a form of an 'N-tuple pendulum' in which each hinge, denoted by a subscript, s, has a positive spring stiffness coefficient, $\tilde{K}_s$, and a positive damping coefficient, $\tilde{C}_s$, associated with it. Figure 2 shows a representation of $(s-1)$th and sth elements of the 'pendulum'.

In order to model the motion of the 'N-tuple pendulum', we form a system of equations using Lagrange mechanics in similar manner to that of Fenlon *et al.* [5, 6]. We must therefore determine the kinetic and potential energies and the non-conservative forces acting on the elements. It is relatively straightforward to show that the kinetic energy T of a filament of N such elements is given by

$$T = \frac{1}{2}\tilde{m}\tilde{l}^2 \sum_{i=1}^{N}\sum_{j=1}^{i-1}\sum_{k=1}^{i-1} \dot{\theta}_j\dot{\theta}_k \cos(\theta_j - \theta_k)$$

$$+\frac{1}{2}\tilde{m}\tilde{l}^2 \sum_{i=1}^{N}\sum_{j=1}^{i-1} \dot{\theta}_i\dot{\theta}_j \cos(\theta_i - \theta_j) + \frac{1}{6}\tilde{m}\tilde{l}^2 \sum_{i=1}^{N} \dot{\theta}_i^2 \tag{4}$$

where θ_s is the angle subtended by the element, s, with respect to the x co-ordinate axis. The potential energy V due to gravitational effects and the stiffness at each element is given by

$$V = \frac{1}{2}\tilde{m}g\,\tilde{l}\sum_{i=1}^{N}(2N - 2i + 1)(1 - \cos(\theta_i)) + \frac{1}{2}\sum_{i=1}^{N}\tilde{K}_i(\theta_i - \theta_{i-1})^2 \tag{5}$$

where the terms due to the stiffness at each hinge are valid only for small values of $\theta_s - \theta_{s-1}\ \forall s$ (and that $\theta_0 = \dot{\theta}_0 = 0$). (Note that the subscript s for the element angles run from 1 to N,

although we may define—notationally only—an angle θ_0 which aids our definition of the potential energy in Equation (5).) Indeed, this is an explicit assumption of our treatment of the filament. We also note that gravity is assumed to work in the (positive) x-direction. The Lagrangian given by $\bar{L} = T - V$ may now be utilised in order to obtain the Euler–Lagrange equations by determining

$$\frac{\mathrm{d}}{\mathrm{d}t}\left(\frac{\partial \bar{L}}{\partial \dot{\theta}_s}\right) - \frac{\partial \bar{L}}{\partial \theta_s} = \tilde{f}_s(\theta_s, \dot{\theta}_s) \tag{6}$$

(Note that the symbol $\bar{L}$ refers to the Lagrangian and that L refers to the dimensional filament length.) The function $\tilde{f}_s(\theta, \dot{\theta})$ represents the externally applied torques exerted on a given element s and these torques are non-conservative. We subdivide the terms within this function into two distinct pieces, given by

$$\tilde{f}_s(\theta_1 \cdots \theta_N, \dot{\theta}_1 \cdots \dot{\theta}_N) = -\tilde{C}_s(\dot{\theta}_s - \dot{\theta}_{s-1}) - \tilde{C}_{s+1}(\dot{\theta}_s - \dot{\theta}_{s+1}) + \frac{1}{2}\tilde{\Delta}_s \tilde{l} \tag{7}$$

The damping terms are thus encoded in the terms $\tilde{C}_s(\dot{\theta}_s - \dot{\theta}_{s-1}) + \tilde{C}_{s+1}(\dot{\theta}_s - \dot{\theta}_{s+1})$, and favour a difference between angular velocities of successive elements (both above and below a particular element s) which is small. A very stiff filament is thus approximated by having large values for both $\tilde{K}_s$ and $\tilde{C}_s$. The term $\tilde{\Delta}_s$ in Equation (7) refers to external forces (distinct from the internal stiffness and damping terms) acting on the filament elements creating a torque of strength $1/2\tilde{\Delta}_s\tilde{l}$, which in this case are due to the fluid pressures forces generated by the (flowing) liquid. For the present case we assume that viscous shear forces acting parallel to the pendulum are negligible.

The Euler–Lagrange equations may be determined analytically, in order to give

$$\begin{aligned}
&\sum_{i=1}^{s-1} \ddot{\theta}_i \cos(\theta_s - \theta_i)\left(N - s + \frac{1}{2}\right) + \sum_{i=s}^{N} \ddot{\theta}_i \cos(\theta_s - \theta_i)\left(N - i + \frac{1}{2}\right) - \frac{1}{6}\ddot{\theta}_s \\
&\quad + \sum_{i=1}^{s-1} \dot{\theta}_i^2 \sin(\theta_s - \theta_i)\left(N - s + \frac{1}{2}\right) + \sum_{i=s}^{N} \dot{\theta}_i^2 \sin(\theta_s - \theta_i)\left(N - i + \frac{1}{2}\right) \\
&\quad + \frac{\tilde{K}_s}{\tilde{m}\tilde{l}^2}(\theta_s - \theta_{s-1}) + \frac{\tilde{K}_{s+1}}{\tilde{m}\tilde{l}^2}(\theta_s - \theta_{s+1}) + \frac{\tilde{C}_s}{\tilde{m}\tilde{l}^2}(\dot{\theta}_s - \dot{\theta}_{s-1}) + \frac{\tilde{C}_{s+1}}{\tilde{m}\tilde{l}^2}(\dot{\theta}_s - \dot{\theta}_{s+1}) \\
&\quad + \left(N - s + \frac{1}{2}\right)\frac{\tilde{g}\sin(\theta_s)}{\tilde{l}} = \frac{\tilde{\Delta}_s}{2\tilde{m}\tilde{l}}
\end{aligned} \tag{8}$$

We should note that our model uses the fact that by definition $\tilde{K}_{N+1} = \tilde{C}_{N+1} = 0$, and hence θ_{N+1} does not contribute to the Euler–Lagrange equations. In order to formulate a more general model, we non-dimensionalise the above Euler–Lagrange equations. We do this by introducing (as before) characteristic scales for mass, length, velocity, and time such that

$$m = \frac{\tilde{m}}{M}; \quad l = \frac{\tilde{l}}{L}; \quad t = \frac{\tilde{t}U_\infty}{L} \tag{9}$$

The quantities $\tilde{K}_s$, $\tilde{C}_s$, and $\tilde{\Delta}_s$ may also be non-dimensionalised in a similar manner to give

$$K_s = \frac{\tilde{K}_s}{U_\infty^2 M}; \quad C_s = \frac{\tilde{C}_s}{U_\infty M L}; \quad \Delta_s = \frac{\tilde{\Delta}_s L}{M U_\infty^2}; \quad g = \frac{\tilde{g} L}{U_\infty^2} \tag{10}$$

The non-dimensionalised Euler–Lagrange equations are now written as

$$\begin{aligned}
&\sum_{i=1}^{s-1} \ddot{\theta}_i \cos(\theta_s - \theta_i)\left(N - s + \frac{1}{2}\right) + \sum_{i=s}^{N} \ddot{\theta}_i \cos(\theta_s - \theta_i)\left(N - i + \frac{1}{2}\right) - \frac{1}{6}\ddot{\theta}_s \\
&+ \sum_{i=1}^{s-1} \dot{\theta}_i^2 \sin(\theta_s - \theta_i)\left(N - s + \frac{1}{2}\right) + \sum_{i=s}^{N} \dot{\theta}_i^2 \sin(\theta_s - \theta_i)\left(N - i + \frac{1}{2}\right) \\
&+ \frac{K_s}{ml^2}(\theta_s - \theta_{s-1}) + \frac{K_{s+1}}{ml^2}(\theta_s - \theta_{s+1}) + \frac{C_s}{ml^2}(\dot{\theta}_s - \dot{\theta}_{s-1}) + \frac{C_{s+1}}{ml^2}(\dot{\theta}_s - \dot{\theta}_{s+1}) \\
&+ \left(N - s + \frac{1}{2}\right)\frac{g \sin(\theta_s)}{l} = \frac{\Delta_s}{2ml}
\end{aligned} \tag{11}$$

We note that the ratio of the density of the soap fluid to that of silk (in the experiment of Zhang *et al.* [1]) has been estimated to be about 0.9. Hence buoyancy terms and thus gravitational terms are small, and we henceforth set g to zero. However, we have not yet considered the effects of coupling the filament to the fluid and the effect that this has on our non-dimensionalisation of the coupled system. The force acting on an element of the filament in the 'dimensional' system in our Euler–Lagrange equations (namely $\tilde{\Delta}_s$) must be related to the pressure difference (between those pressures acting on the 'bottom', $\tilde{p}_s^{\text{bottom}}$, and the 'top', $\tilde{p}_s^{\text{top}}$, of a filament element) such that

$$\begin{aligned}
&\delta \tilde{p}_s = \tilde{p}_s^{\text{bottom}} - \tilde{p}_s^{\text{top}} \\
&\Rightarrow \tilde{\Delta}_s = \tilde{l}\,\delta \tilde{p}_s
\end{aligned} \tag{12}$$

The non-dimensional form of this equation is given by

$$\Delta_s = \left(\frac{\rho_f L^2}{M}\right) l \delta p_s = \mathrm{Fl}\,\delta p_s \tag{13}$$

where ρ_f is the two-dimensional density of the fluid. Furthermore, we note that we may express the mass of the filament in the experimental (dimensional) system in terms of the linear density of the filament σ, where $M = \sigma L$. The dimensionless variables describing the behaviour of a single filament in a flowing two-dimensional soap bubble are given by Equation (10) along with

$$R_e = \frac{L \rho U_\infty}{\mu}; \qquad F = \frac{\rho_f L}{\sigma} \tag{14}$$

We assume that coefficients $\tilde{K}_s$ and $\tilde{C}_s$ are dimensioned properties of the filament which are thus independent of the length L of the filament in the experiment.

The numerical algorithm uses the equations of motion above of Equation (11) in order to cast the problem into a matrix equation for the angular accelerations, given by

$$M\ddot{\theta} = p(\theta, \dot{\theta}) \tag{15}$$

We note that the matrix M has elements $M_{s,i}$, where

$$\begin{aligned} M_{s,i} &= \cos(\theta_s - \theta_i)\left(N - s + \frac{1}{2}\right); \quad i < s \\ M_{s,i} &= \left(N - s + \frac{1}{3}\right); \quad i = s \\ M_{s,i} &= \cos(\theta_s - \theta_i)\left(N - i + \frac{1}{2}\right); \quad i > s \end{aligned} \tag{16}$$

The right-hand side of the matrix equation thus has elements $p_s(\theta, \dot{\theta})$ given by

$$\begin{aligned} p_s(\theta, \dot{\theta}) = &-\sum_{i=1}^{s-1} \dot{\theta}_i^2 \sin(\theta_s - \theta_i)\left(N - s + \frac{1}{2}\right) - \sum_{i=s}^{N} \dot{\theta}_i^2 \sin(\theta_s - \theta_i)\left(N - i + \frac{1}{2}\right) \\ &- \frac{K_s}{ml^2}(\theta_s - \theta_{s-1}) - \frac{K_{s+1}}{ml^2}(\theta_s - \theta_{s+1}) - \frac{C_s}{ml^2}(\dot{\theta}_s - \dot{\theta}_{s-1}) \\ &- \frac{C_{s+1}}{ml^2}(\dot{\theta}_s - \dot{\theta}_{s+1}) + \frac{\Delta_s}{2ml} \end{aligned} \tag{17}$$

The matrix M is inverted to produce an explicit representation of the accelerations

$$\ddot{\theta} = M^{-1} p(\theta, \dot{\theta}) \tag{18}$$

Hence, we may thus determine the angular accelerations, for example by using numerical method such as LU decomposition, if we know all of the angles and angular velocities at a particular time. We note that the matrix M never became singular in any of the simulation runs that were performed. However, if such a case were to occur then standard singular-value decomposition techniques would be used.

The values for the angular accelerations are thus determined at a particular time t once both the angles and angular velocities are known for each element. These accelerations and velocities are used to determine the element angles and angular velocities at time $t+\delta t$ by using Runge–Kutta integration. LU decomposition algorithms determine the angular accelerations at time $t + \delta t$ and this process is repeated until we have determined the filament's asymptotic behaviour with respect to time.

We note the Euler–Lagrange equations are themselves quite 'stiff' and so we utilized a standard adaptive step sizing algorithm for δt in order to maintain the accuracy of the Runge–Kutta method at all points during our simulation. The sum of the error in all of the element angles and their angular velocities is set to be 10^{-8} in these calculations. This set of equations has been tested and compared with the trivial $N = 1$ system as well as the $N = 3$ system [7], for the case of $\tilde{\Delta}_1 = 0$. Using an arbitrary starting point at $t = 0$ for the angles and their angular velocities and arbitrary values for the stiffness and damping coefficient, the difference in solutions was negligible for values of $t \leqslant 50$.

Note that the non-dimensional width of the filament, $2\delta\varepsilon$, was set at 0.04 and that this value is in agreement with the experimental situation [1]. The results presented in this article are preliminary and do not constitute an exhaustive survey of the stability of our solution as the simulation parameters were altered or indeed of the behaviour of the model as a function of the parameters K_s, C_s, and Re, etc. However, we note that the results did not significantly change qualitatively when we increased the fineness of the mesh and/or increased the number of filament elements, N. (The interested reader is also referred to related articles of Fenlon *et al.* [5, 6] which used a similar N-tuple pendulum approach in order to study the behaviour of leaflets in artificial heart valves and dealt with the question of the numerical accuracy of this method in detail.) Indeed, we may also note that identification of a single oscillating case as a function of K_s, C_s, and Re, etc., and determination of both filament and fluid properties—as well as reducing the filament 'effective length' (see below)—was a highly non-trivial problem, even without a detailed study of the numerical accuracy of our solution. This present study outlines our technique and initial results which we believe capture much of the essential physics of this system, although we intend to carry out further calculations which will study the numerical accuracy of our approach, the suitability of our Lagrangian model, and the behaviour of this complex and highly coupled system in more detail. The results of these calculations will be presented in another article.

Values for the parameters

In order to carry out the simulations and compare with experiments by Zhang *et al.* [1], values for the parameters K_s, C_s, Re, and F need to be determined as a function of L. Experimental values for the kinematic viscosity are given by $\nu = \mu/\rho = 4 \times 10^{-4}\,\mathrm{m^2 s^{-1}}$ and the linear density of the filament $\sigma = 2 \times 10^{-5}\,\mathrm{kg\,m^{-1}}$ [1] give a value for the characteristic velocity as U_∞ of $3\,\mathrm{m\,s^{-1}}$, we thus find that

$$K_s = 5.5 \times 10^3 \tilde{K}_s L^{-1}; \quad C_s = 1.7 \times 10^4 \tilde{C}_s L^{-2}; \quad F = 175L$$

Given that L lies in the range [0.02,0.06] then F must lie in the range [3, 10]. By contrast, it is much more difficult to determine the values for K_s and C_s because we have no definitive values for the dimensionalised quantities. However, we choose values for both K_s and C_s which produce results from our simulations consistent with the results of experiment [1]. It is found that reasonable results are obtained for $\tilde{K}_s < 10^{-2}$ and $\tilde{C}_s < 10^{-2}$. (We furthermore make an explicit assumption that the effects of damping are roughly as important as those of stiffness.) The value for the elasticity of silk (namely, $E \leqslant 65\mathrm{N\,m^{-2}}$) may be used to obtain a rough value for $\tilde{K}_s$ and this value is found to be consistent with the values used in our calculation.

By re-writing the non-dimensional quantities given in Equation (10) we then have

$$K_s = \frac{\tilde{K}_s}{U_\infty^2 \sigma L}; \qquad C_s = \frac{\tilde{C}_s}{U_\infty \sigma L^2} \tag{19}$$

with σ the linear material density. If the length of the filament is altered the corresponding non-dimensional coefficients also change. Most notably if the length L is reduced then the filament becomes effectively 'stiffer' and more 'damped'. Conversely by increasing the length the filament becomes 'soft' and underdamped. We note that the non-dimensional damping parameter C_s changes non-linearly with length.

Filament boundary and initial conditions

With reference to Figure 2 implicit in the Euler–Lagrange equation set is the fact that $\theta_0 = 0$ and plays no part in the calculations although θ_1 may be non-zero. We should note however that the potential in the stiffness terms would wish to make $\theta_1 \to 0$, that is along the direction of flow. It is an interesting test to see whether alternative vortex formulations could be formed when a zero imposition is placed on θ_1. Early indications with heart valve simulations studies suggest that the effect is not large.

It is crucial to impose initial conditions which do not lie in or too close to either of the 'attracting basins' (namely, the oscillating and non-oscillating modes) when determining the interface between stationary and oscillatory states. Hence initial conditions for the filament, in all presented cases, were such that $\theta_s \neq 0; \dot{\theta}_s = 0 \ \forall s$; at $t = 0$. In order to obtain stable solutions for the Navier–Stokes equations the initial conditions were enforced for 5 time steps. The filament was then 'released' and made to move under the influence of the fluid forces as described below.

THE FLUID/STRUCTURE INTERACTION ALGORITHM

The solution algorithm for the fluid/structure interaction consists of

- At time $t = 0$ a position and velocity of each of the elemental filaments is assumed known. The initial filament position $(x_i(0), y_i(0))$ is then 'mapped' onto the CFD mesh. This entails assuming a finite width of the filament, $2\delta\varepsilon$, centred about the filament elements, and finding the velocity nodes n_{veli} which are positioned inside the strip $(x_i \pm \delta\varepsilon \sin\theta_i, y_i \pm \delta\varepsilon \cos\theta_i)$ as shown in Figure 3.
- These velocity nodes, n_{veli}, are then flagged as prescribed boundary conditions using the velocities of the nearest filament centre $(\dot{x}_i(t), \dot{y}_i(t))$ which essentially models the fluid 'no-slip' condition.
- The Navier–Stokes equations (Equation (3)) using the outer boundary conditions (as shown in Figure 1) and imposing the prescribed motion of the filament at time t (as described immediately above) are iteratively solved over a small time interval δt.
- Since the pressure profile imposes its magnitude throughout the boundary layer nodes in the finite element mesh used to evaluate the pressure force acting on the filament surface are taken from within the same fluid domain as the velocity vector. These are indexed and averaged along the filament element. The number of pressure nodes for each element can vary from a minimum of three upwards, depending on the ratio of finite element size to filament size. The pressure difference as given by Equation (12) is then evaluated and used as part of the non-conservative forces in the Euler Lagrange equations of Equation (11).
- The Euler–Lagrange matrix equation of Equation (18) is solved over the small time period δt.
- The position of the elemental filaments is updated to $(x_i(t + \delta t), y_i(t + \delta t))$.
- And the time is updated to $t_{\text{new}} = t_{\text{old}} + \delta t$.
- The process is repeated until time the reaches some large predefined value (30 non-dimensional seconds was found to be adequate).

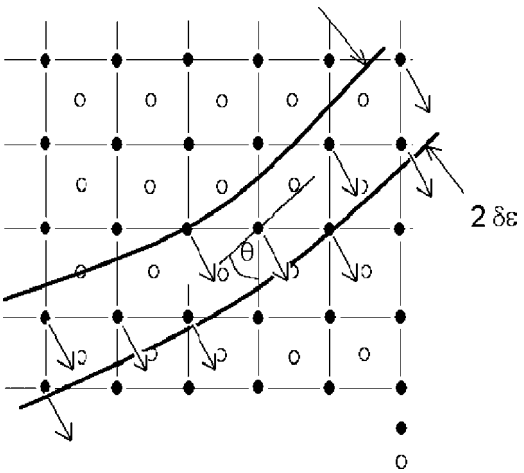

Figure 3. Representation of the filament 'mapped' onto the computational mesh with constrained degrees of freedom.

This interaction algorithm is termed the 'fictitious domain' method and is essentially a weakly coupled process. Note that the pressures are sampled within a given distance both above and below the filament (and not *in* the filament) and an average pressure value acting at each filament element was determined. A distance of twice the thickness of the filament $\delta\varepsilon$ was used and this seemed to provide good results. A fuller treatment of varying the distance in which the pressures acting on the filament elements are determined will be carried out in future and the results of this treatment will be presented elsewhere.

RESULTS AND DISCUSSION

A specific case of an oscillating filament

We now wish to identify a stable oscillating state for the filament containing only a 'single wavelength' with respect to position along the length of the filament, closely mirroring the situation seen in the experiment [1]. The number of elements, $N = 10$, was found to be quite large enough in order to adequately simulate the properties of the filament. (Increasing N made little or no difference to the solution, although we note that future calculations will consider the effects of varying N in more rigour—as mentioned above.) The parameter K_s appeared to have the largest effect in the number of wavelengths along the length of the filament. As K_s increased, and the filament becomes stiffer, we found that the number of wavelengths along the length of the filament was reduced. As mentioned above, we therefore chose a value specifically for K_s which produced a single wavelength with respect to the length of the filament as was observed in experiment [1]. We also found that reasonable results were obtained for values of C_s which were of approximately the same or smaller magnitude than

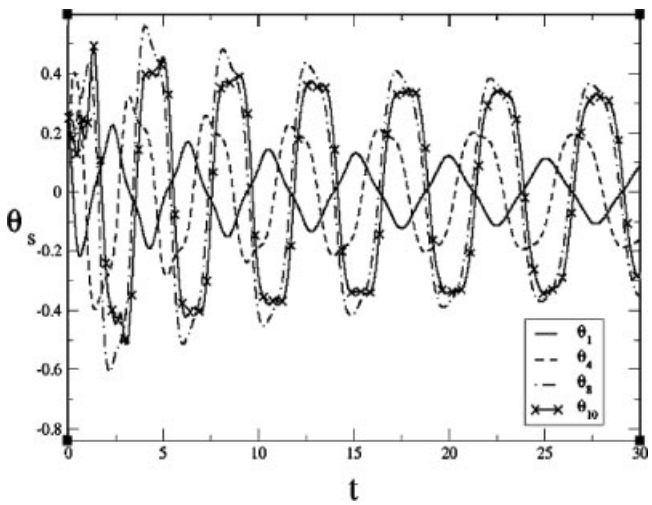

Figure 4. Results for the element angles for a single filament in an oscillatory mode of effective length (see text for details) of $S = 1.0$.

K_s. In this manner, we obtained a value for the stiffness coefficient of $K_s = 0.013$ and adequate results were obtained for $C_s = 0.0025$. Furthermore, we chose 'typical' values for F and for the Reynolds number of $F = 1$ and of $Re = 500$, respectively. It is important to note that we wish only to produce a single case in the 'phase space' of these parameters, which we know to be oscillating. We will use these values as *reference* values when we wish to reduce the effective length of the filament thus driving the system from an oscillatory to a non-oscillatory phase and we denote this value of L as L_{ref}. We may now also define a dimensionless quantity S (which we shall also refer to as the 'effective length') which represents changes in the length of the filament with respect to this reference value, where $S = L/L_{\text{ref}}$. We therefore argue that at this stage of the algorithm development it is quite reasonable to choose these parameters for the oscillatory state in such a heuristic manner, as long as we are rigorous later on when we alter the effective length of the filament. Again, we note that a fuller investigation of varying all parameters, including the effective length S, will be carried out elsewhere.

Figure 4 shows the angular time evolution of three of the $N = 10$ elements making up the filament. We clearly see that the motion of the filament is oscillating and that the amplitude of these oscillations is constant, thus indicating a stable oscillatory state.

We furthermore note that the amplitude of oscillations is much larger than our initial angles at $t = 0$ indicating that the filament has drawn energy from the fluid. The period of the oscillation also remains constant for approximately $t > 10$. We analyse this more quantitatively by performing a Fourier transform of the angle element time series. Figure 5 shows the Fourier transform of the time series for four of the element angles.

Using the experimental values of viscosity, a filament length of 0.03 m and inlet velocity of $3\,\text{m}\,\text{s}^{-1}$, we clearly see a strong fundamental mode at about $f = 0.2$, which corresponds to a dimensional value of about 20 Hz, which is slightly lower than the experimental result of

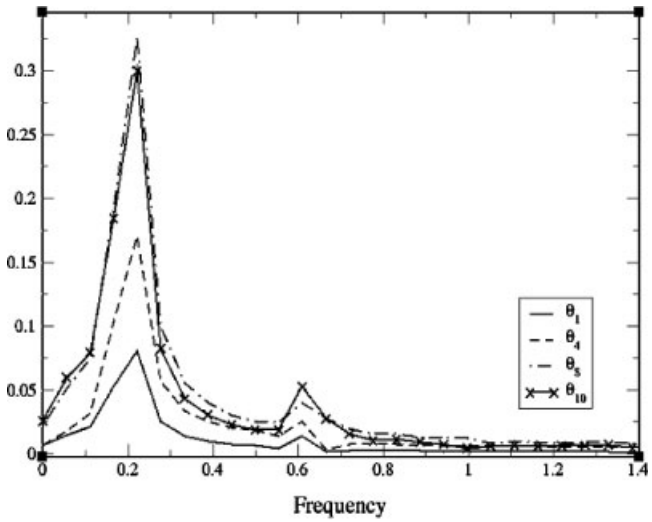

Figure 5. Results for the fourier transform of the time series for the element angles plotted against frequency (non-dimensionalised) for a single filament in an oscillatory mode of effective length $S = 1.0$.

50 Hz [1]. We note that we primarily wish to prove the principle that we are able to adequately simulate an oscillating filament, although we note that, in principle, we are able to choose values of our parameters (including the pressure boundary conditions) which would provide a fundamental frequency of 50 Hz in dimensional units, as seen in experiment. However the parameter space of, at the minimum, four variables is large given the computational effort required for each time-dependent solution.

Animations generated from the numerical time-dependent results show that, for the case where a single wavelength is present along the filament (the fundamental mode), the effective bluff body shape of the leading edge of the filament induces boundary layer separation as normal. Two small recirculation zones exist and if the body were non-deforming then these recirculation zones would be shed periodically. However since the filament is deformable, as one of the recirculation zones starts to grow the asymmetric pressure profile (measured between upper and lower surfaces of the filament) induces a curvature in the filament itself. This allows two competing phenomena: firstly, the recirculation zone on the side of concave curvature grows and this induces further curvature of the filament; and secondly, the recirculation zone on the opposite side is effectively trapped by the convexity of the deforming filament. Hence only one vortex is allowed to develop at a time and this vortex is convected along the length of the filament at the wave-speed of the filament curvature. We note that during this convection period the curvature of the filament essentially 'follows' the motion of the recirculation zone. This tends to suggest that the flapping is essentially a 'lock-in' phenomenon [8]. However, although the Strouhal number can be used to represent vortex induced vibration for non-deformable bodies, the Strouhal number may not be used here because the body is deformable. The vortices are enhanced by the curvature of the filament (a function of the parameters K_s and C_s), which are (in a circular fashion) created by the existence of the vortex itself. Hence we can see that energy is being given to the filament from the fluid by

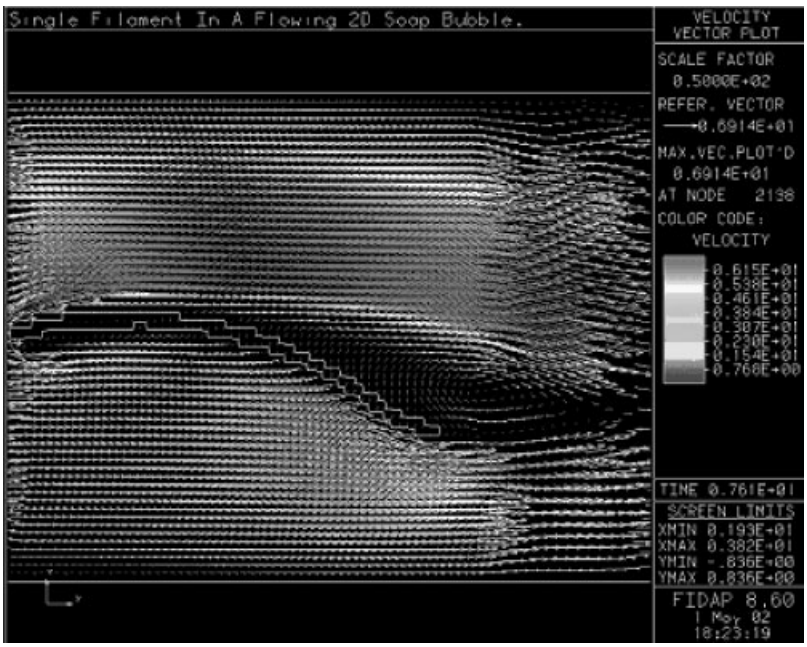

Figure 6. Filament and velocity vectors plotted for a 'typical' profile for the oscillating filament.

virtue of the generation and enhancement of the recirculation zones. This phenomenon is very similar to that seen in Reference [9] where oscillating foils have their highest efficiency when a leading edge vortex is convected downstream and coalesces with the trailing edge vortex to cause a reverse Kármán street, indicating that the fundamental flapping mode corresponds to the minimal energy state.

Figure 6 shows the velocity vector field for a 'typical' filament profile with the presence of a single vortex being shed from the upper part of the filament trailing edge whilst a small recirculation zone is being formed at the lower leading edge of the filament.

Behaviour of the system with varying effective length

Experiments showed [1] that the oscillatory motion may be completely extinguished for low enough values of the filament length. In order to ratify the numerical model we reduce the effective length S of the filament whilst keeping all other parameters (such as the viscosity of the liquid, $\tilde{K}_s$, and $\tilde{C}_s$) constant. We do this by choosing a new value for $S(<1)$ and then by using Equations (9), (10) and (14). K_s and C_s now both increase in magnitude, whereas both Re and F decrease. We would thus expect that all of these effects would tend, at the very least, to reduce the amount of oscillation of the filament, if not completely destroy any oscillations.

Note that our initial flapping state, governed by the parameters given above, can be expressed in terms of our 'effective' length, $S(=1.0)$. Thus, $S=0.2$ or 0.5 corresponds to a fifth or a half of the original length respectively. Figure 7 now shows the time variation for the element at the trailing edge of the filament for values of $S=0.2$, 0.5, 0.75 and 1.0.

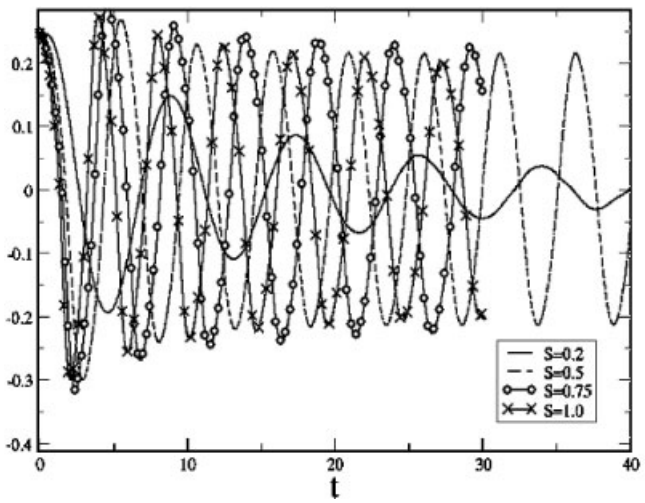

Figure 7. Results for the y-value of the trailing edge of the filament plotted against time in seconds (non-dimensionalised) for varying values of the effective length S.

We note that in order to be as consistent with the experimental situation as possible we increase the width of the computational domain as we decrease S (although the length of the computational domain remains constant). This ensures that the numerical simulations take account of the effects of the outer (rigid, no slip) boundaries when the motion of the filament is of the order of the width, h, of the soap film. Thus, the computational problem becomes much more intensive as we reduce S due to reducing the individual mesh element size. We assume that the aspect ratio of the filament remains the same however.

The amplitude of the non-dimensional oscillations for $S = 0.5$ are about the same as for $S = 1.0$ so that the amplitude of the oscillations in the dimensional system for $S = 0.5$ are about half that of $S = 1.0$. The $S = 0.2$ case shows a much smaller amplitude and indeed this simulation is near to the boundary of our capability computationally due to the increasing size of the mesh with corresponding decreased length. This might be adequately resolved by using parallel processing techniques, although this remains the subject of future research. We note that in this case the filament covers, at most, two nodal mesh points, and the asymptotic motion of the filament with respect to time cannot be seen by the naked eye in our animations due to the coarseness of the mesh. However, we still believe that the simulation results clearly indicate that this case does indeed oscillate for $S = 0.2$, albeit (as mentioned above) with a very small amplitude. We note that, although the mesh nodes which lie within the filament may not change for large values of time, the imposed velocities at these nodes clearly do change and that this is enough to form a stable oscillatory state. However, we are probably very close to the boundary of critical damping for $S = 0.2$ and we are clearly capturing some of the essential physics of this complex and strongly coupled system.

By contrast, we may start from an initial configuration for the filament in which all element angles and element velocities are zero and the filament is thus initially aligned with respect to the fluid flow. Our results show that this mode is found to be stable (i.e. non-oscillating) over

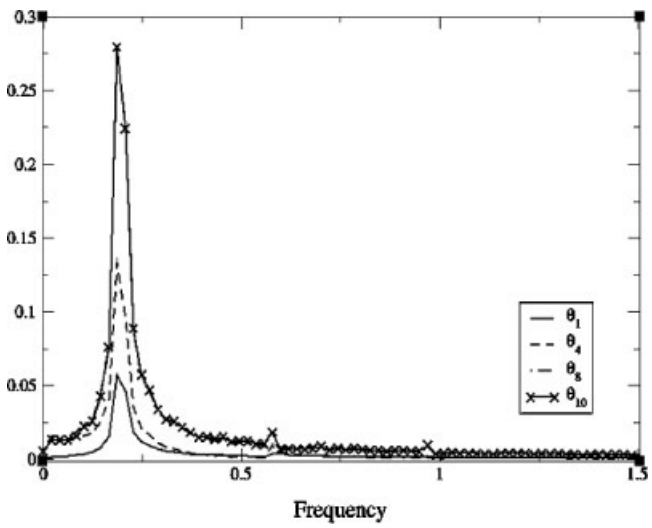

Figure 8. Fourier transform of time evolution of the element angles as a function of non-dimensional frequency and for an effective length of $S = 0.5$.

a large area of our parameter space. For example, we find that this configuration is stable for values of our parameters which correspond to $S = 1$ and above. We strongly believe however that this 'mode' would become unstable (begin to oscillate) as we decrease the values for the stiffness and damping and we increase the Reynolds number in which case small pressure differences along the length of the filament would be enough to 'perturb' the system into an oscillating (or even a chaotic) mode. Indeed, this would correspond to increasing the dimensional length of the filament and this effect was observed in experiment. Again, a detailed investigation into this phenomenon will given in another article.

Figures 5, 8, and 9 show the Fourier transform versus non-dimensional frequency for various element angles corresponding to $S = 1.0$, 0.5 and 0.2, respectively. The fundamental frequency seems to be inversely proportional to the length of the filament for the cases in which the amplitude of oscillation is large (namely, $S = 1.0$, 0.75, and 0.5), although more data is needed to confirm this. It is in contrast to that found for a lateral vibration of a bar of length L fixed at $x = 0$ and free at $x = L$ where the frequency is inversely proportional to L^2 [10].

In addition, this is contrary to experimental evidence [1] where the flapping frequency was measured to be independent of filament length. However, it is unclear whether the fluid velocity remained constant as the filament length was changed in these experiments. The finite boundaries of the soap film may well have had a significant influence on the characteristic velocity for various filament lengths, especially for large motion of the free end.

For the $S = 0.2$ case, shown in Figure 9, where the flapping amplitude is very small, the non-dimensional fundamental frequency during the transient phase is lower than that for $S = 1.0$ and 0.5. Also additional frequency modes are apparent, although this may be a function of the transitory phase before oscillations begin to die out.

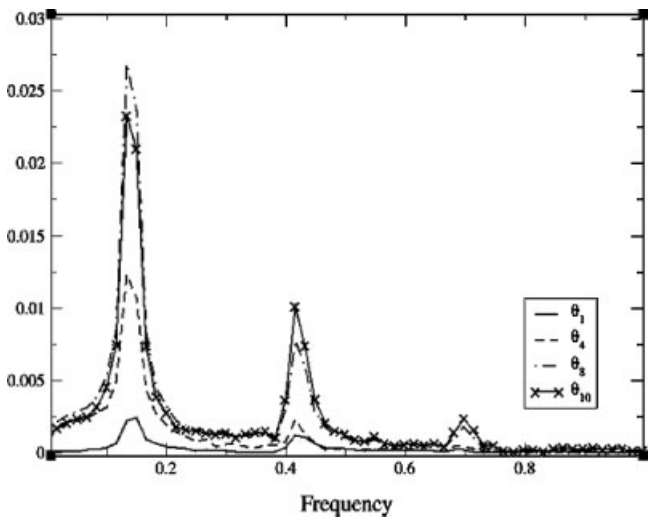

Figure 9. Fourier transform of time evolution of the element angles as a function of non-dimensional frequency and for an effective length of $S = 0.2$.

Experiments in the soap films seem to show that the vortices released from the trailing edge are much smaller than the amplitude of oscillation. This is not seen in our numerical simulations. In fact for the numerical simulation the vortices are clearly derived from the amplitude of oscillation as they are convected downstream (see Figure 6).

The Reynolds number quoted by Zhang *et al.* [1] for the soap film experiments is of the order of 10^4. We note however that the figures in Reference [1] clearly showed vortical structures emanating from the trailing edge of the filament, which furthermore clearly indicates a laminar flow. It has been noted [11] that some 3D instabilities normally associated with turbulence (roll instabilities in 3D Couette flow) are completely suppressed by the soap film hydrodynamics. This suppression of flow phenomena may also be occurring for the experiments but is not simulated in the numerical experiments. In the experiments no vortical structures are seen which are convected downstream from the leading to trailing edge. This may be due to the vorticity that is generated in the viscous boundary layer being constrained by the surface tension forces to lie in the domain where surface tension dominates. They are only released when, at the trailing edge, the pressure difference can overcome the surface tension. It is noted however that the vortical structures do seem to be released at similar positions to that found in 'true' fluid flow [11] for non-deforming bodies, in which the characteristic diameter is larger than that found with the silk filament.

As noted by Martin and Wu [4] the surface viscosity tends to dominate the fluid flow phenomena in soap films. The fluid flow profiles seem to be that normally seen with considerably lower Reynolds numbers, although Reynolds numbers evaluated from the bulk viscosity given in Reference [4] are high. This may again be due to the dominance of the surfactant layer surface viscosity. It has proved extremely difficult to ascertain the exact corresponding Reynolds number for a numerical simulation of the flow in a soap film. This will need significant further investigation.

CONCLUSIONS

We have simulated the properties of the time-dependent fluid structure interaction of a thin filament in a 2D flowing fluid by using the 'fictitious domain' method. The mesh used in the computational algorithm is stationary, although large amplitude motion of solid bodies are observed. This is in contrast to other methods where the mesh moves with solid boundaries, an example of which can be found in Reference [12]. The motion of the filament is gross and there are no assumptions concerning the ratio of filament motion to that of filament length. The numerical simulations support experimental of Zang *et al.* [1] evidence that two stable states exist. We have identified a stable mode in which the filament is seen to oscillate. We may reduce the effective length of the filament and the initial oscillations are seen to be strongly suppressed. By contrast to the experiment, vortical structures are developed at the leading edge and they are preferentially grow within the curvature of the filament. These vortices are subsequently convected downstream and are released at the trailing edge. As in the experiments, the sign of the released vortex alternates with the direction of the oscillation. We note that the fluid forces exerted on the filament in the numerical simulation are due to pressure only. This effect has been seen in the experiments [1] where the 'flapping' motion is limited to about two wavelengths of the 'free' end for a long filament.

Clearly, many more investigations will be needed to study the numerical accuracy of our procedure in detail, although we note here that refinement of our mesh and increasing the number N of elements in the filament was not seen qualitatively to affect our results greatly. We note that many of the problems associated with the numerical stability of our procedure were extensively studied previously in related work for artificial heart values of Fenlon *et al.* in References [5, 6]. We would also wish to further map out the behaviour of this strongly coupled system as a function of parameters such as Reynolds number, stiffness and damping terms, boundary condition, and the 'effective length' of the filament. We would also wish to determine the extent of the viscous force acting parallel to the filament. It would also be highly desirable to carry out simulations for simulation parameters that are clearly in the 'overdamped' regime. We would expect the oscillations to die away completely in this case. However, we note that our simulations are clearly capturing some of the essential physics occurring in this system, and that the simulations presented in this article constitute a highly non-trivial computational problem.

ACKNOWLEDGEMENTS

This work was funded under EPSRC grant number GR/M35154.

REFERENCES

1. Zhang J, *et al.* Flexible filaments in a flowing soap film as a model for one-dimensional flags in a two-dimensional wind. *Nature* 2000; **408**:835–839.
2. Rutgers MA, *et al.* Two-dimensional velocity profiles and laminar boundary layers in flowing soap films. *Physics of Fluids* 1996; **8**(11):2847–2854.
3. Chomaz JM, Cathalau B. Soap films as two-dimensional classical fluids. *Physical Review A* 1990; **41**(4):2243–2245.
4. Martin B, Wu X-I. Shear flow in a two-dimensional Couette cell: A technique for measuring the viscosity of free standing liquid films. *Review of Scientific Instruments* 1995; **66**(12):5603–5608.
5. Fenlon AJ, David T. Numerical models for the simulation of flexible leaflet heart valves Part 1—computational methods. *Computer Methods in Biomechanics and Biomedical Engineering* 2001; **4**(4):323–39.

6. Fenlon AJ, David T. Numerical models for the simulation of flexible leaflet heart valves Part 2—valve studies. *Computer Methods in Biomechanics and Biomedical Engineering* 2001; **4**(6):449–462.
7. Erikkson R. *Problems Using Mathematica*. Wiley: New York, 1994.
8. Blevins RD. *Flow-induced Vibrations.* van Nostrand: Princeton, NJ, 1977.
9. Anderson JM, *et al*. Oscillating foils of high propulsive efficiency. *Journal of Fluid Mechanics* 1998; **360**:41–72.
10. Timoshenko S, Young DH. *Vibration Problems in Engineering*. Van Nostrand: New York, 1955.
11. Peschard I, Le Gal P. Coupled wakes of cylinders. *Physical Review Letters* 1996; **77**(15):3122–3125.
12. Leuprecht A, *et al*. Numerical study of hemodynamics and wall mechanics in distal end-to-side anastomoses of bypass grafts. *Journal of Biomechanics* 2002; **35**(2):225–36.

